Electronic Supplementary Information

Electrodepositing 3D porous rGO electrode for efficient hydrogel electrolyte integration towards 1.6 V flexible symmetric supercapacitors

Kaizheng Song, [# a] Yuqi Jiang, [# b] Xiang Pang, [a] Yuanyuan Li,[*,c] Jinping Liu[* a, b]

[a] School of Chemistry, Chemical Engineering and Life Science, Wuhan University of Technology, Wuhan, 430070, Hubei, China. E-mail: liujp@whut.edu.cn

[b] State Key Laboratory of Advanced Technology for Materials Synthesis and Processing, Wuhan University of Technology, Wuhan, 430070, Hubei, China.

[c] School of Optical and Electronic Information, Huazhong University of Science and Technology, Wuhan, 430074, Hubei, China. Email: liyynano@hust.edu.cn

# These authors contributed equally to this work.

Experimental section

Synthesis of 3D rGO film on SS

rGO film was synthesized using electrodeposition method. Before electrodeposition, 40 mg GO was firstly added to 0.1 M $NaClO_4$ solution. Then, the mixture was processed by ultrasonic cell disruptor for 30 minutes at room temperature, making the tightly stacked GO layers in the mixture dispersed. The electrodeposition was performed on a CS310 electrochemical workstation by using a traditional three-electrode configuration. In detail, the SS, platinum sheet (Pt) and saturated calomel electrode (SCE) were utilized as the working electrode, counter electrode and reference electrode, respectively. For the growth, constant voltage polarization mode at -1.2 V was carried out for 15 hours, with the GO reduced to rGO, forming a film with 3D porous networks (0.15 mg cm^{-2}; the loading mass can be readily controlled by changing the polarization time). After the reaction, the sample was taken out, rinsed with deionized water for several times. Finally, the flexible 3D rGO@SS electrode was obtained after freeze drying for 48 h in vacuum freeze dryer.

Assembly of symmetric supercapacitor (SC) device

Firstly, the $NaClO_4$-PVA sol electrolyte was prepared as follows: 4 g PVA 1799 (Aladdin Biochemical Technology, Shanghai, China), 5.6 g $NaClO_4$ were added into 40 mL deionized water and further heated to 80 ^oC under vigorous stirring until the solution became clear. Then, two pieces of 3D rGO@SS electrodes (1 cm^2) were soaked in the sol electrolyte for 5 minutes and consequently assembled face-to-face under a pressure and left overnight until the sol electrolyte was solidified into gel. The gel electrolyte also served as the separator.

Characterizations

The morphology and structure of the as-prepared electrode sample was characterized by SEM (Phenom ProX, 10.0 kV) and XRD (Bruker D-8 Advance) with Cu Kα irradiation (λ=1.54 Å). XPS measurements were performed with Thermo Scientic

K-Alpha using monochromatic Al Ka radiation to analyze the surface composition of rGO@SS electrode. Raman spectra were collected from Witech CRM200 Raman spectrometer using 632.8 nm He-Ne laser.

Electrochemical measurements

All the electrochemical measurements were performed on a CS310 Electrochemical Workstation at ambient temperature. Electrodes' property testing was performed in a three-electrode electrochemical system. The 3D rGO@SS was cut into small pieces (1 cm^2 of active area) and utilized directly as the working electrode, while Pt plate and saturated calomel electrode (SCE) were used as the counter electrode and the reference electrode, respectively. The electrolyte was 1 M Na_2SO_4 aqueous solution (40 mL). Areal capacitance of the electrode (C_s, mF cm^{-2}) was calculated based on the equation:[1]

$$Cs = \int idV / 2Sv \triangle V$$

where $\int idV$ is the integrated CV area, S is the geometrical area of the electrode, v is the scan rate, and $\triangle V$ is the voltage window.

The electrochemical impedance spectroscopy (EIS) data of the device was collected using an Autolab electrochemical working station, with an AC voltage of 5 mV amplitude in the frequency range from 100 kHz to 0.1 Hz.

The areal capacitance of the symmetric SC (C_{cell}, mF cm^{-2}) was calculated by the equation:[2]

$$C_{cell} = I \times \triangle t / (\triangle V \times S)$$

where I, $\triangle t$, $\triangle V$ and S are the current, discharging time, voltage window and the geometrical area of the electrode, respectively. The areal/volumetric energy and power densities were calculated based on the following equations:[2]

$$E = \frac{\int IV(t)dt}{A}$$

$$P = E / \triangle t$$

Where I is the discharging current, $V(t)$ is discharging voltage at t, dt is time differential, Δt is the total discharging time, and A is the device's area or volume.
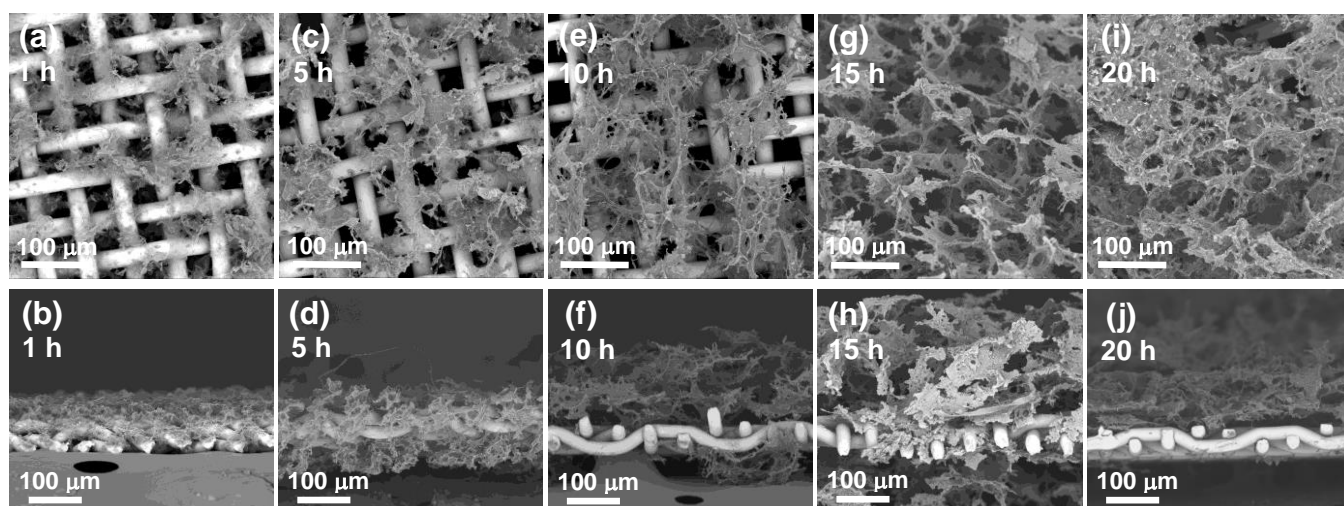
Figure S1. SEM images of the rGO@SS electrodes prepared with different deposition times. The thickness of the rGO film increases steadily from 70 to 400 μm when the electrodeposition time is prolonged from 1 to 15 h. However, the thickness is only ~320 μm after 20 h electrodeposition, which is probably due to the partial exfoliation of the very thick film.
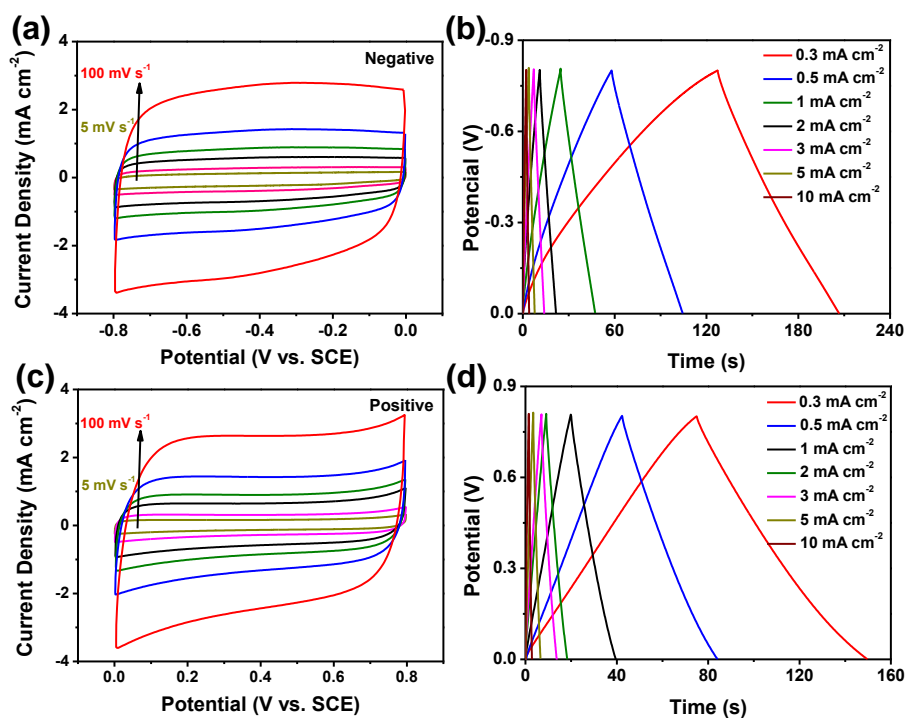
Figure S2. (a) CVs and (b) GCD curves of the rGO@SS as negative electrode. (c) CVs and (d) GCD curves of the rGO@SS as positive electrode.
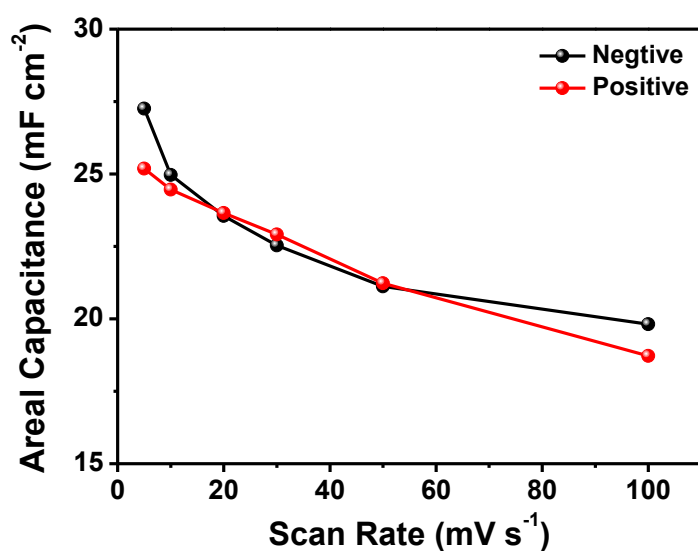

Figure S3. Comparative areal capacitances at various scan rates (5-100 mV s⁻¹) of the positive and negative electrodes.
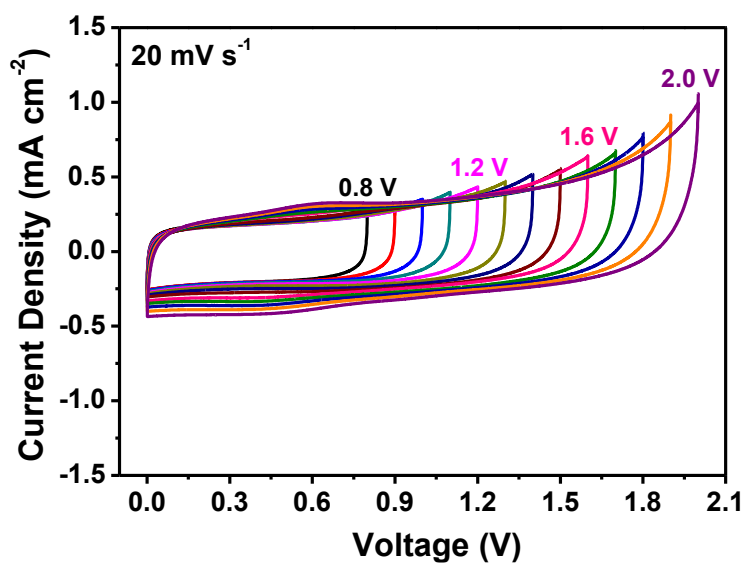
Figure S4. CV curves of the 3D rGO-based SC device with different voltage windows at 20 mV s^{-1}.

Table S1. Comparison of voltage window of the 3D rGO-based SC with other carbon-based SCs.

| Electrode material	Electrolyte	Voltage window	Reference
Graphene–carbon nanosphere	6 M KOH	1.2 V	3
CNT	PVA/H_3PO_4	0.8 V	4
Activated carbon cloth	PVA/H_2SO_4	1.0 V	5
Activated carbon	PVA/KOH	1.0 V	6
Graphene	PVA/H_2SO_4	1.0 V	7
Graphene sheets	PVA/H_2SO_4	0.8 V	8
rGO/PPy	PVA/H_2SO_4	0.8 V	9
Graphene	PVA/H_2SO_4	1.0 V	10
MWCNTs	PVA/H_3PO_4	0.8 V	11
rGO/PANI	PVA/H_2SO_4	1.0 V	12
3D rGO	**1 M Na_2SO_4 PVA/$NaClO_4$**	**1.6 V**	**this work**
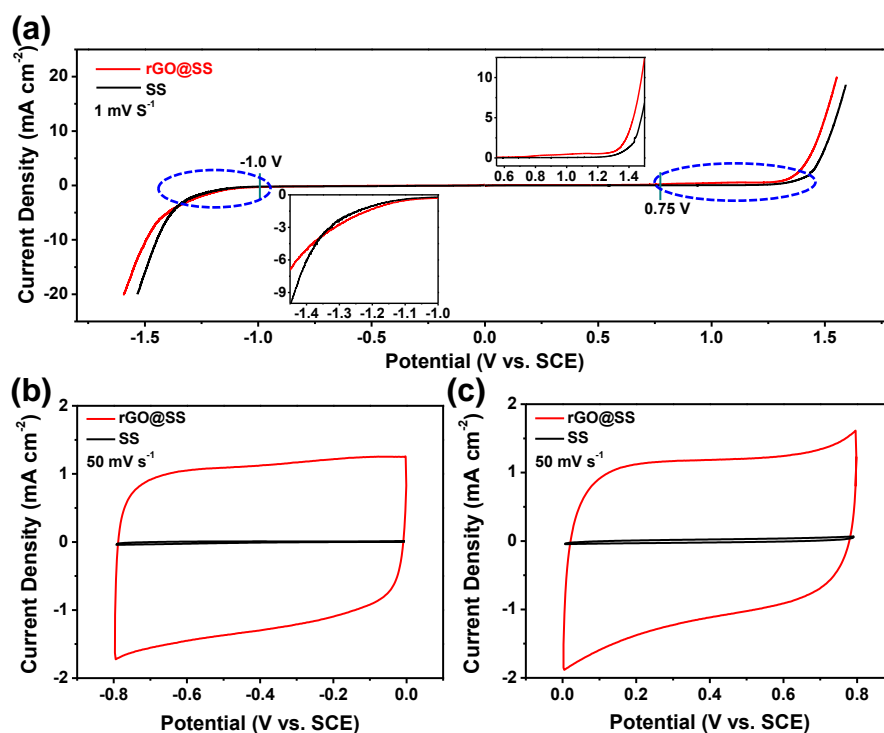
Figure S5. (a) LSV curves of SS and rGO@SS. (b-c) CV curve comparison of the SS and rGO@SS electrodes. In Na_2SO_4 aqueous electrolyte, the potentials for oxygen evolution reaction and hydrogen evolution reaction on rGO@SS electrode are ~0.75 V and -1.0 V, respectively. From Figure S5a, it is found that the overpotential for oxygen evolution reaction on SS is higher than rGO@SS, while the overpotential for hydrogen evolution reaction on rGO@SS is higher than SS. Therefore, the origin of this overpotential increase should come from the combination effect of SS and rGO. In addition, based on previous report[13], the lower contents of H^+ and OH^- in Na_2SO_4 electrolyte compared with acidic and alkaline electrolytes are very helpful to achieve higher overpotentials for hydrogen and oxygen evolution.
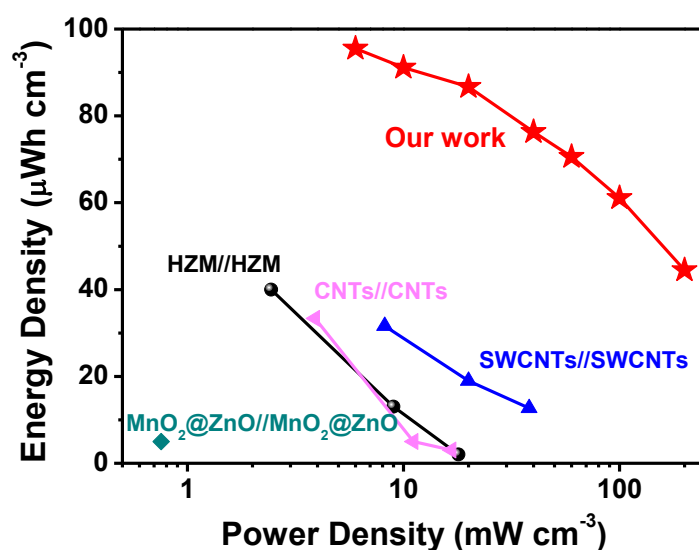
Figure S6. Volumetric Ragone plot of the quasi-solid-state device. At high power density of 200 mW cm^{-3}, the device still has an energy density of 44.45 μWh cm^{-3}, which is obviously superior to many reported supercapacitors based on hydrogenated single-crystal ZnO@amorphous ZnO-doped MnO$_2$ core-shell nanocable (HZM, 40 μWh cm^{-3} at 2.44 mW cm^{-3}), single-walled carbon nanotubes (SWCNTs, 31.6 μWh cm^{-3} at 8.18 mW cm^{-3}), MnO$_2$-coated ZnO nanowires (MnO$_2$@ZnO, 5.0 μWh cm^{-3} at 0.756 mW cm^{-3}), and carbon nanotubes (CNTs, 33.36 μWh cm^{-3} at 3.892 mW cm^{-3}). [14-17]
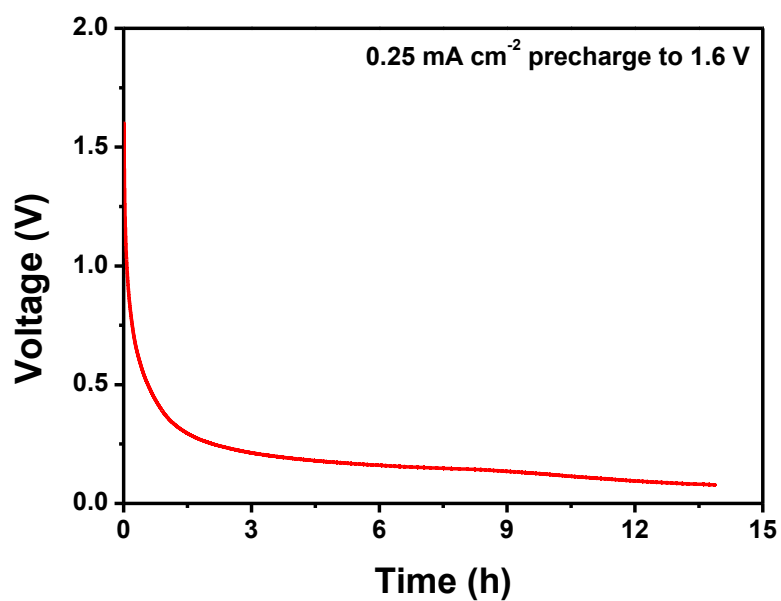
Figure S7. The self-discharging curve of the quasi-solid-state device. The device has a self-discharge time of ∼15 h (from V_{max} to 0).
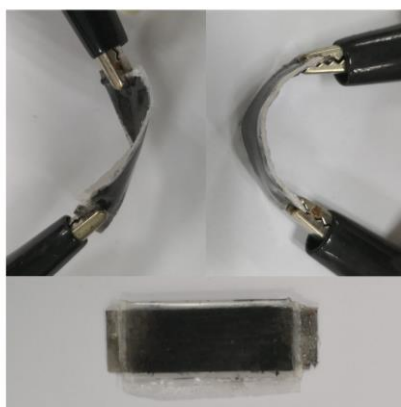

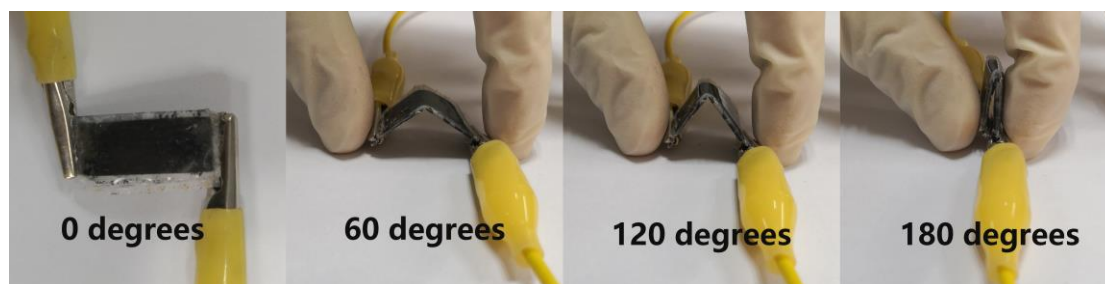**Figure S8.** Digital photographs showing the flexibility of the device.

Figure S9. Digital photographs of the 3D rGO-based SC device under different bending situations.

References

1. Y. Zou, Q. Wang, C. Xiang, Z. She, H. Chu, S. Qiu, F. Xu, S. Liu, C. Tang and L. Sun, *Electrochim. Acta*, 2016, **188**, 126-134.
2. Z. S. Wu, Y. Zheng, S. Zheng, S. Wang, C. Sun, K. Parvez, T. Ikeda, X. Bao, K. Müllen and X. Feng, *Adv. Mater.*, 2017, **29**, 1602960.
3. N. Díez, M. Qiao, J. L. Gómez-Urbano, C. Botas, D. Carriazo and M. M. Titirici, *J. Mater. Chem. A*, 2019, **7**, 6126-6133.
4. M. Liao, H. Sun, J. Zhang, J. Wu, S. Xie, X. Fu, X. Sun, B. Wang and H. Peng, *Small*, 2018, **14**, 1702052.
5. S. Jiang, T. Shi, X. Zhan, H. Long, S. Xi, H. Hu and Z. Tang, *J. Power Sources*, 2014, **272**, 16-23.
6. D. Zhao, C. Chen, Q. Zhang, W. Chen, S. Liu, Q. Wang, Y. Liu, J. Li and H. Yu, *Adv. Energy Mater.*, 2017, **7**, 1700739.
7. J. Yu, J. Wu, H. Wang, A. Zhou, C. Huang, H. Bai and L. Li, *ACS Appl. Mater. Interfaces*, 2016, **8**, 4724-4729.
8. K. Parvez, Z. S. Wu, R. Li, X. Liu, R. Graf, X. Feng and K. Müllen, *J. Am. Chem. Soc.*, 2014, **136**, 6083-6091.
9. X. Liu, T. Qian, N. Xu, J. Zhou, J. Guo and C. Yan, *Carbon*, 2015, **92**, 348-353.
10. A. Ramadoss, K. Y. Yoon, M.-J. Kwak, S. I. Kim, S. T. Ryu and J.-H. Jang, *J. Power Sources*, 2017, **337**, 159-165.
11. L. Liu, D. Ye, Y. Yu, L. Liu and Y. Wu, *Carbon*, 2017, **111**, 121-127.
12. F. Chen, P. Wan, H. Xu and X. Sun, *ACS Appl. Mater. Interfaces*, 2017, **9**, 17865-17871.
13. K. Fic, G. Lota, M. Meller, E. Frackowiak, *Energy Environ. Sci.*, 2012, **5**, 5842-5850.
14. P. Yang, X. Xiao, Y. Li, Y. Ding, P. Qiang, X. Tan, W. Mai, Z. Lin, W. Wu, T. Li, H. Jin, P. Liu, J. Zhou, C. P. Wong and Z. L. Wang, *ACS Nano*, 2013, **7**, 2617-2626.
15. M. Kaempgen, C. K. Chan, J. Ma, Y. Cui and G. Gruner, *Nano Lett.*, 2009, **9**, 1872-1876.
16. J. Bae, M. K. Song, Y. J. Park, J. M. Kim, M. Liu and Z. L. Wang, *Angew. Chem. Int. Ed.*, 2011, **50**, 1683-1687.
17. Y. J. Kang, H. Chung, C.-H. Han and W. Kim, *Nanotechnology*, 2012, **23**, 065401.